



Broadband efficient anomalous reflection using an aggressively discretized metasurface

CHU QI AND ALEX M. H. WONG*

State Key Laboratory of Terahertz and Millimeter Waves, Department of Electrical Engineering, City University of Hong Kong, Hong Kong

*alex.mh.wong@cityu.edu.hk

Abstract: Aggressive discretization in metasurface design—using the least number of unit cells required—can dramatically decrease the phase coverage requirement, thus allowing the use of simple structure and avoiding unit cells with strong resonance, leading to a simple design with broadband performance. An aggressively discretized metasurface with two unit cells per period can realize efficient anomalous reflection. In this work, we investigate the power efficiency and bandwidth of an aggressively discretized metasurface featuring anomalous reflection. Through spectral domain considerations, we find that the theoretical upper limit for the bandwidth of this metasurface reflecting all the incident power into the desired mode is 67%. With aggressive discretization, we design a metasurface with a simple unit cell structure. By tuning the two unit cells, we achieve a metasurface design that reflects more than 80% of the incidence power into the desired anomalous reflection mode over a broad bandwidth of 53.6%. Such bandwidth is unprecedented for an anomalous reflection metasurface. Finally, we fabricate and experimentally demonstrate our anomalous reflection metasurface and obtain bandwidth and efficiency performances which agree well with simulation.

© 2022 Optica Publishing Group under the terms of the [Optica Open Access Publishing Agreement](#)

1. Introduction

As a 2-D artificial material, metasurfaces have been attracting research interest because of their versatile manipulation of electromagnetic (EM) waves, including wave redirection, polarization control and beamforming, among numerous other applications. [1–26]. Most metasurfaces are designed with fine discretization, which means they are constructed with many subwavelength unit cells, mimicking a gradual change of phase/impedance response along the surface [4,13–24]. For a finely discretized metasurface design, the electrically small unit cell size (typically about one-tenth of a wavelength) may cause fabrication difficulty, especially at high frequencies. The design process of finding a large number of unit cells to achieve full phase/impedance coverage can be complicated. Sometimes one may need to use unit cells with strong resonance, which will compromise the power efficiency and bandwidth. Generally, the bandwidths of finely discretized metasurfaces are limited due to the resonant nature of the subwavelength-sized unit cells. For example, M. Chen, *et al.* proposed a bianisotropic metasurface to realize reflectionless wide-angle refraction. The 3-dB power efficiency bandwidth of this refraction metasurface is 4% [20]. In a following work [21], they used the wire-loop structure — a more natural implementation of a Huygens' source — for the bianisotropic metasurface design to achieve a wider bandwidth. They realized 95% normalized anomalous refraction power efficiency (ratio between power coupled into the desired mode and the total power scattered from the metasurface) across a bandwidth of 3.5%. However, the structure featured a dissipative loss of 16% - hence over the said bandwidth the anomalous reflection power efficiency (the ratio between the power carried by the anomalously reflected wave and that carried by the incident wave) is about 80%-84%. In [22], the authors proposed a Huygens' metasurface for smaller refraction angles and realized a 3-dB power efficiency bandwidth of 8%. Reflection metasurface designs can use simpler structure due to decreased diffraction modes, which can potentially lead to broader bandwidth. The reflectors

proposed in [23] and [24] can realize efficient wide-angle reflection with 3-dB bandwidths of 5% and 7%.

Recently, researchers have proposed the concept of metagrating [27–33]. By designing each period as a scatterer, it is possible to use simple structures and alleviate the problems caused by electrically small feature size in the finely discretized metasurface design. R. Oshri, *et al.* have proposed a metagrating that can anomalously reflect more than 90% of the incident power into the desired mode within a frequency bandwidth up to 21% [27]. However, most existing metagrating designs aim at maximizing anomalous scattering efficiency at one frequency, which may limit their bandwidth performance [28–32]. Besides, it is essentially difficult to control the bandwidth performance when one designs the period of a metasurface as a whole.

In parallel, our group has proposed the concept of the aggressively discretized metasurface [34–36]. By designing a metasurface with the least number of unit cells required, one can use a very simple structure and avoid unit cells with strong resonance. Aggressive discretization in metasurface design can potentially lead to efficient and broadband performance. Work [34], for example, presented a bipartite Huygens' metasurface (two unit cells per period) which achieves near-perfect anomalous reflection at a single design frequency, and a 90% power efficiency over a bandwidth of 25.7%. While [34–36] pursued maximized efficiencies at the design frequency, it is of practical importance to pursue designs where the bandwidth is maximized while the power efficiency remains respectable.

In this work, we investigate the theoretical and practical bandwidth limitations for an aggressively discretized metasurface featuring anomalous reflection. After establishing a theoretical upper limit on the bandwidth of the metasurface, we proceed to design a metasurface with wideband performance which attains, as much as possible, the theoretical upperbound. By properly tuning the metasurface unit cells, we arrive at a metasurface design which achieves anomalous reflection with a power efficiency of 80% or higher over a bandwidth of 53.6%. This bandwidth is roughly doubled from known anomalous reflection metasurfaces, including metagratings and previous aggressively discretized metasurfaces, which greatly extends the practical application realms of the metasurface.

2. Design formulation: aggressively discretized metasurface realizing anomalous reflection

We use the k -space operation to describe the diffraction mechanism of a periodic metasurface. Figure 1(a) shows the k -space operation of a periodic metasurface with period Λ_g illuminated by a plane wave with incident angle θ_i . The reflection spectrum will consist of an infinite number of diffraction modes, of which the n^{th} diffraction mode will have a tangential wave number of

$$k_n = k_i + nk_g, \quad (1)$$

where

$$k_i = k_0 \sin \theta_i \text{ and } k_g = \frac{2\pi}{\Lambda_g}. \quad (2)$$

Of the infinite number of diffraction modes, the ones within the propagation range $[-k_0, k_0]$ can scatter into the far field while the ones outside the propagation range are evanescent. Figure 1(b) is a schematic of the reflective metasurface in (a), with the reflection angles depicted in Fig. 1(c). The reflection angle of the n^{th} propagating diffraction mode can be determined using

$$\theta_{r,n} = \sin^{-1} \frac{k_n}{k_0}. \quad (3)$$

In the k -space operation, the structure of the metasurface and its interaction with the incoming EM wave will determine the amplitude and phase of each diffraction mode. We use array theory to analyze the diffraction modes generated by a periodic metasurface.

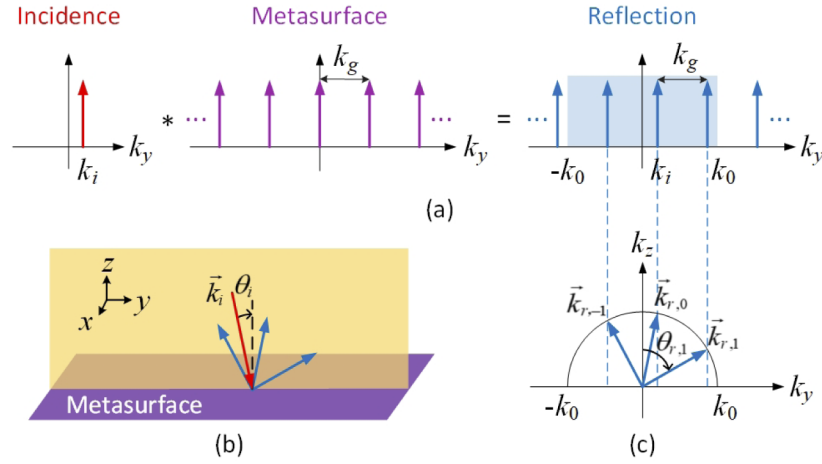


Fig. 1. (a) k -space operation of a periodic metasurface which varies along the y -direction. Arrows indicate the existence of diffraction modes. The blue box in the reflection spectrum denotes the propagation range of $[-k_0, k_0]$. (b) A schematic of the reflective metasurface in (a) upon an incidence with wave number \bar{k}_i and incident angle θ_i . (c) An angular representation of the reflection spectrum in (a), $\bar{k}_{r,n}$ ($n = -1, 0, 1$) are the wave numbers of n^{th} diffraction modes.

Consider a periodic metasurface with M unit cells per period, the m^{th} unit cell has a complex reflection coefficient r_m , where $m = 1, \dots, M$. In the spatial domain, the reflection coefficients along the metasurface is discrete with spacing Λ_g/M between adjacent unit cells and periodic with M unit cells. As a property of the Fourier transform, in the spatial frequency domain the diffraction modes will be discrete with interval $k_g = 2\pi/\Lambda_g$ between adjacent diffraction modes and periodic of M diffraction modes. Denoting r_m and \tilde{r}_n as Fourier series pairs, we have

$$r_m = \sum_{n=0}^{M-1} \tilde{r}_n e^{jn \frac{2\pi}{M} m},$$

$$\tilde{r}_n = \frac{1}{M} \sum_{m=0}^{M-1} r_m e^{-jn \frac{2\pi}{M} m}.$$
(4)

From (4) we know that the coefficient of the n^{th} diffraction mode is \tilde{r}_{-n} . We have shown in a previous work that a metasurface with a discretization level of N cells per period is sufficient for tuning N propagating modes in the reflection spectrum [34]. That is, to realize control over N propagating modes, the most aggressive discretization level is $M = N$.

Therefore, to design an aggressively discretized metasurface realizing a desired anomalous reflection with θ_i and θ_r , we can use the k -space operation to determine the metasurface period (Λ_g) and the number of propagating diffraction modes (N). With aggressive discretization, the number of unit cells per period is $M = N$. In this case, the unit cell size along the variation (y) direction is $U_y = \Lambda_g/N$. After describing the desired reflection spectrum through the set of \tilde{r}_n 's, we can use (4) to calculate the required reflection coefficients of the unit cells. Finally, we design the unit cells with the required reflection coefficients and combine them to form the metasurface.

We have shown in [34] that often the desired anomalous reflection can be achieved with only two propagation modes—a 0^{th} mode for specular reflection and a -1^{st} mode for anomalous reflection (assume $k_i > 0$). In such cases, we can realize efficient anomalous reflection using a bipartite metasurface, i.e., a metasurface with a discretization level of two unit cells per period. The anomalous reflection is achieved by suppressing the specular (0^{th}) mode and redirecting all

the power into the anomalous reflection (-1^{st}) mode. That is, we should design the reflection coefficients of the two metasurface unit cells $\{r_1, r_2\}$ to realize $\{\tilde{r}_0 = 0, \tilde{r}_1 = 1\}$. From the first line of (4) we have

$$\begin{cases} r_1 = \tilde{r}_0 + \tilde{r}_1 e^{j\pi} = -1, \\ r_2 = \tilde{r}_0 + \tilde{r}_1 e^{j2\pi} = 1. \end{cases} \quad (5)$$

That is, the required reflection coefficients of the two unit cells should have the same (unitary) reflection magnitude with a 180° reflection phase difference.

Figure 2(a) shows the k -space operation of a bipartite metasurface realizing anomalous reflection. For an incident wave from an angle θ_i and with tangential wave number of $k_i \in (0, k_0)$, the anomalous reflection appears at the -1^{st} diffraction order, which has a tangential wave number of $k_{r,-1} = k_i - k_g$, thus the reflection angle can be expressed as

$$\theta_r = \sin^{-1} \frac{k_i - k_g}{k_0}. \quad (6)$$

Figure 2(b) is a schematic of the metasurface in Fig. 2(a), with its reflection angles depicted in Fig. 2(c).

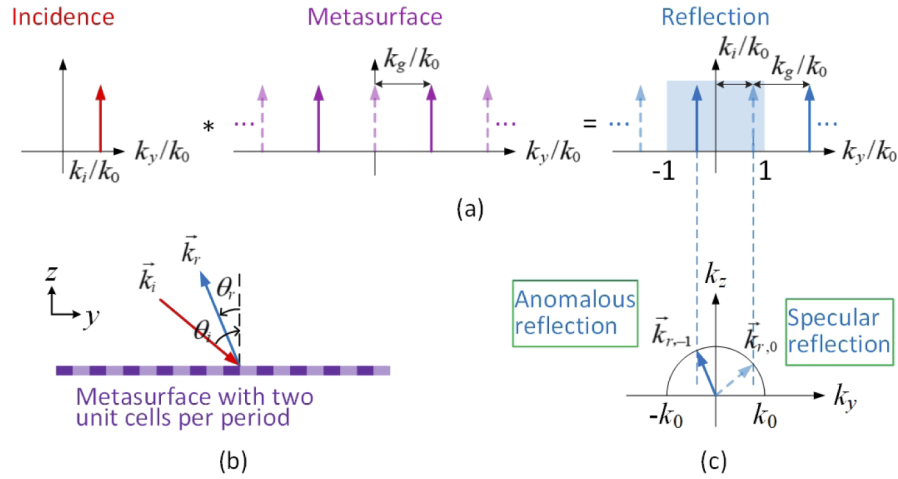


Fig. 2. (a) k -space operation of a periodic metasurface realizing anomalous reflection. The metasurface has a discretization level of two unit cells per period. Arrows with solid (dashed) lines represent diffraction modes with non-zero (zero) amplitude. The wave numbers are normalized to k_0 . (b) A schematic of the reflective metasurface in (a). (c) An angular representation of the reflection spectrum in (a).

3. Bandwidth investigation

3.1. Theoretical bandwidth upper limit of a bipartite metasurface realizing anomalous reflection

In the reflection spectrum of Fig. 2(a), the tangential wave numbers (normalized to k_0) of -1^{st} and -2^{nd} diffraction modes are

$$\begin{cases} k_{r,-1}/k_0 = k_i/k_0 - k_g/k_0 = \sin \theta_i - \frac{c}{\Lambda_g f} \\ k_{r,-2}/k_0 = k_i/k_0 - 2k_g/k_0 = \sin \theta_i - \frac{2c}{\Lambda_g f}, \end{cases} \quad (7)$$

where c and f are the light velocity and frequency. We can see that $k_{r,-1}/k_0$ and $k_{r,-2}/k_0$ will increase with increasing f . Then the cut-off frequencies (f_1 and f_2) can be calculated:

$$\begin{cases} k_{r,-1}/k_0 = -1 \Rightarrow f_1 = \frac{c}{\Lambda_g(1+\sin\theta_i)} \\ k_{r,-2}/k_0 = -1 \Rightarrow f_2 = \frac{2c}{\Lambda_g(1+\sin\theta_i)}. \end{cases} \quad (8)$$

The cut-off frequencies f_1 and f_2 represent frequencies above which the respective modes enter the propagation range. At $f < f_1$, only the 0th mode lies within the propagation range; at $f_1 < f < f_2$, two modes (the 0th and -1st modes) are within the propagation range; at $f > f_2$, at least three modes (the 0th, -1st and -2nd modes) lie within the propagation range. The ideal operation bandwidth, then, is $f_1 < f < f_2$, where two well-tuned unit cells suffice to control both propagation modes [34]. Suppressing the 0th mode effectively channels all the power into the anomalous reflection mode. From (8) we can see, $f_2 = 2f_1$, that is, the percentage bandwidth from f_1 to f_2 is 67%, which is the theoretical bandwidth upperbound for a bipartite reflection metasurface.

3.2. Broadband metasurface design

We then design an aggressively discretized metasurface to achieve efficient anomalous reflection with a broadband performance. Following [34] (to facilitate a direct comparison), we design the metasurface to realize anomalous reflection with $\theta_r = -22.5^\circ$ upon an incidence with $\theta_i = 50^\circ$ at 24 GHz. The same design procedure can be followed for an arbitrary set of $\{\theta_i, \theta_r\}$, though in some cases, such as those involving normal incidence or reflection, a discretization level of $M \geq 3$ may be required. Using (1)–(3), the desired anomalous reflection can be realized with a metasurface with $k_g = k_0 \sin\theta_i - k_0 \sin\theta_r = 1.15k_0$. The corresponding period is $\Lambda_g = 2\pi/k_g = 0.87\lambda_0$, which is 10.88 mm. With a discretization level of two unit cells per period, we then determine the unit cell size along the variation direction (y-direction), which is $U_y = 5.44$ mm. We choose $U_x = U_y = 5.44$ mm to design the metasurface unit cells. Figure 3(a) shows the geometrical structure of the unit cell we use. It is a ground-backed dipole with length L and width W . This simple unit cell structure has been shown to work well over a relatively large angular range and bandwidth [34,35]. We design the unit cell on a Rogers RO4003C board ($\epsilon_r = 3.55$, $\delta_t = 0.0027$) with a substrate thickness of 1.524 mm and copper layer thickness of 17.8 μm . In this work we design for the TE polarization, with the electric field polarized along the x-direction (i.e. E_x, H_y, H_z are non-zero). Notwithstanding, the proposed design formulation is not limited to a certain polarization, by using TM-polarized [35] or dual-polarized [37–39] unit cell structures, metasurface designs for other polarization applications can be achieved. We perform EM simulations using the software Ansys HFSS. Dielectric and conductor losses have been included.

For the unit cell design, by sweeping the dipole length L , we can obtain the unit cell's reflection characteristics under the desired plane-wave incidence, as shown in Fig. 3(b). As we can see, with changing L , the magnitude of the reflection coefficient remains above 95%, and the phase of the reflection coefficient changes gradually, covering a phase range of close to 300° . One may notice that for $2 \text{ mm} < L < 3.5 \text{ mm}$, there is a dip in the reflection magnitude, and the reflection phase changes rapidly with L , which means in this range the unit cell may be more resonant. Strong resonance of some unit cells may lead to limited bandwidth of the metasurface.

To implement the bipartite metasurface described in Section 2, we choose two unit cells with 180° reflection phase difference (as found from (5)) to construct the period of the metasurface. The geometrical structure is shown in Fig. 4(a). We can choose different pairs of unit cells (with dipole lengths of L_1 and L_2) to construct the metasurface. Figure 4(b) shows the anomalous reflection power efficiencies of metasurfaces with different pairs of (L_1, L_2) , where $L_1 < L_2$. The anomalous reflection power efficiency is the ratio between the powers in the anomalously reflected wave (-1st diffraction mode) and the incident wave. We can observe that for different dipole

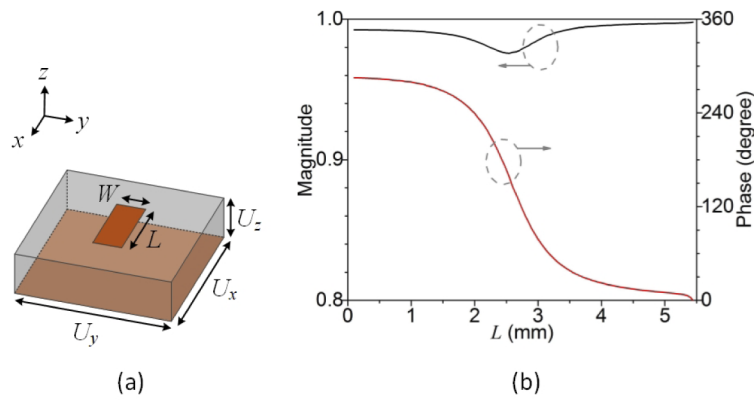


Fig. 3. (a) Geometrical structure of the unit cell. (b) The simulated reflection coefficient (magnitude and phase) of the unit cell as a function of L . Other geometrical parameters are $U_x = U_y = 5.44$ mm, $U_z = 1.524$ mm, $W = 1.0$ mm.

length pairs, the efficiencies are the same at the design frequency of 24 GHz. However, the efficiency within the frequency band (15.6–31.2 GHz) will vary with changing parameters. The lower and upper cut-off frequencies (15.6 GHz and 31.2 GHz), due to the change of the number of diffraction modes within the propagation range, are observed as stipulated by (8).

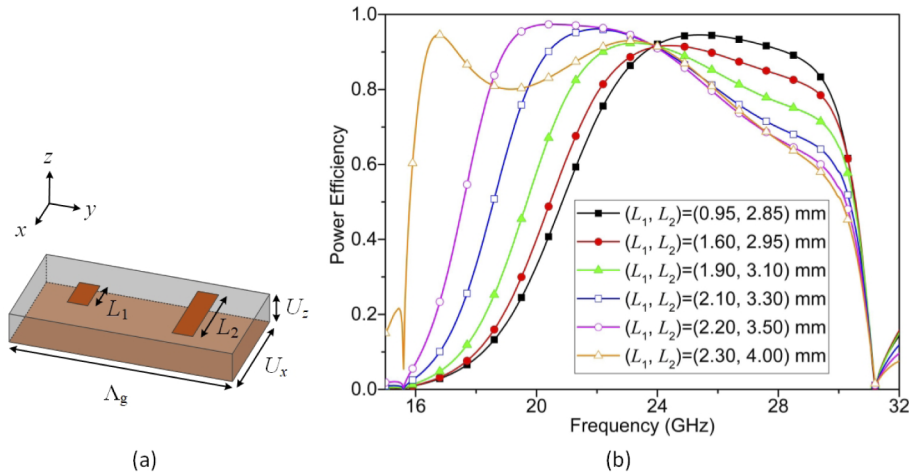


Fig. 4. (a) Geometrical structure of one period of the proposed metasurface. (b) Simulated anomalous reflection power efficiency of the metasurface with different pairs of (L_1, L_2) .

We tune the reflection resonances (controlled respectively by the values of L_1 and L_2) and observe the corresponding effect on anomalous reflection power efficiency over the bandwidth stretching from 15.6–31.2 GHz. Figure 5(a) shows the efficiencies of metasurfaces with different values of L_1 , while L_2 is fixed to 3.7 mm. We observe that the efficiency performance near the lower cut-off frequency (15.6 GHz) remains unchanged; the efficiency near the center frequency improves with increasing L_1 . However, when L_1 is larger than 1.8 mm, the efficiency near the higher cut-off frequency (31.2 GHz) will worsen with increasing L_1 . Figure 5(b) shows the efficiencies of metasurfaces with different values of L_2 , while L_1 is fixed to 1.8 mm. We can see that the efficiency near the higher cut-off frequency remains unchanged, but the efficiency for the lower frequency portion changes, with larger a L_2 in general boosting the efficiency at

the lower frequencies, at the expense of the efficiency near the center frequency. In general, when L_1 and L_2 are tuned such that their resonant frequencies are separated from each other, the bandwidth can be widened. However, the middle part of the efficiency curve will drop because the reflection phase difference of the two unit cells will increasingly deviate from 180° at the central frequencies. Balancing these trends, we tune both L_1 and L_2 to arrive at a broadband, high efficiency anomalous reflection metasurface.

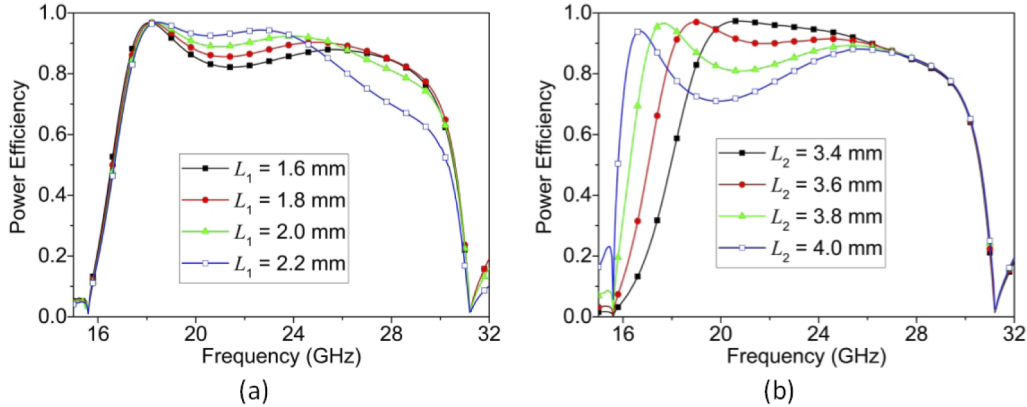


Fig. 5. (a) Simulated anomalous reflection power efficiency of the metasurface with different L_1 while L_2 is fixed to 3.7 mm. (b) Simulated anomalous reflection power efficiency of the metasurface with different L_2 while L_1 is fixed to 1.8 mm.

We choose two unit cells with $L_1 = 1.8$ mm and $L_2 = 3.8$ mm to construct the proposed metasurface, which can achieve an anomalous reflection power efficiency of higher than 80% over a frequency bandwidth of 53.6% (16.8–29.1 GHz). Figure 6 shows the reflection coefficients of the two unit cells. We can see that, within the frequency band of 16.8–29.1 GHz, the two unit cells have near unity reflection coefficients with around 180° reflection phase difference. Figure 7(a) plots the achieved anomalous reflection power efficiency of the proposed metasurface. Figure 7(b) is the normalized scattering of a finite metasurface at different frequencies, showing the beam squinting effect. Equation (6) can be used to calculate the anomalous reflection angles at different frequencies, which are -49.9° , -33.1° , -22.5° and -14.7° at 18 GHz, 21 GHz, 24 GHz and 27 GHz respectively.

3.3. Experiment and discussion

We fabricate and measure the proposed metasurface. Figure 8(a) shows the fabricated metasurface. The size of the fabricated metasurface is 282.9×282.9 mm² (52×52 unit cells). Figure 8(b) shows the experimental setup. In the experiment, the transmitting antenna and the metasurface are fixed upon a rotation stage with the rotation axis aligned to the center of the metasurface. The receiving antenna fixed to the ground effectively measures the wave scattered to an angle θ from the normal direction of the metasurface. Rotating the measurement stage measures the reflection strength as a function of θ .

Figure 9(a) shows the measured anomalous reflection power efficiencies compared with the simulation results. The power efficiency is measured by comparing the scattering peak of the metasurface to that of a same-sized metallic plate. As we can see, the measured power efficiencies agree with the simulated results over the 80% power efficiency band. Figure 9(b) shows the measured scattering patterns of the metasurface at frequencies of 18 GHz, 21 GHz, 24 GHz and 27 GHz, respectively, comparing with those of the same-sized metallic plate. As we can see from

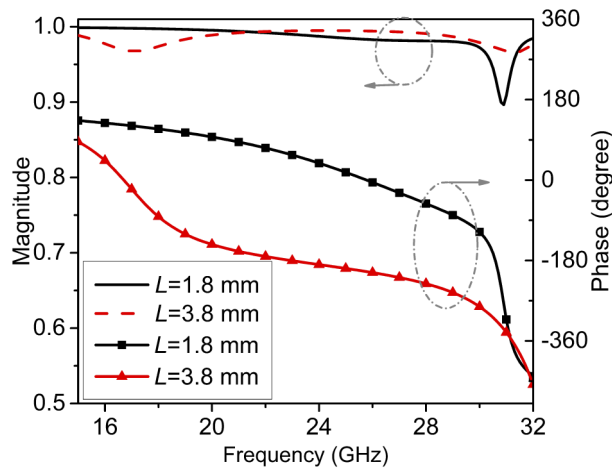


Fig. 6. Simulated reflection coefficients (magnitudes and phases) of the unit cells composing the proposed broadband metasurface.

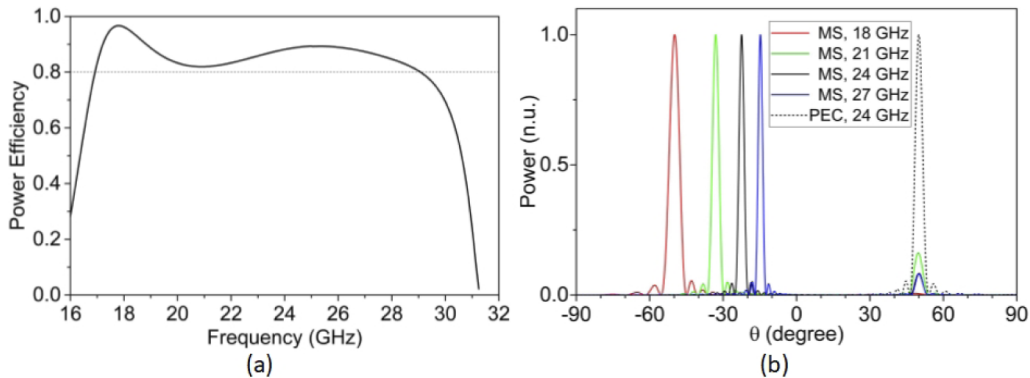


Fig. 7. (a) Simulated anomalous reflection power efficiency of the proposed metasurface. (b) Simulated normalized scattering of a finite metasurface at different frequencies compared with the normalized scattering of a same-sized metallic plate.

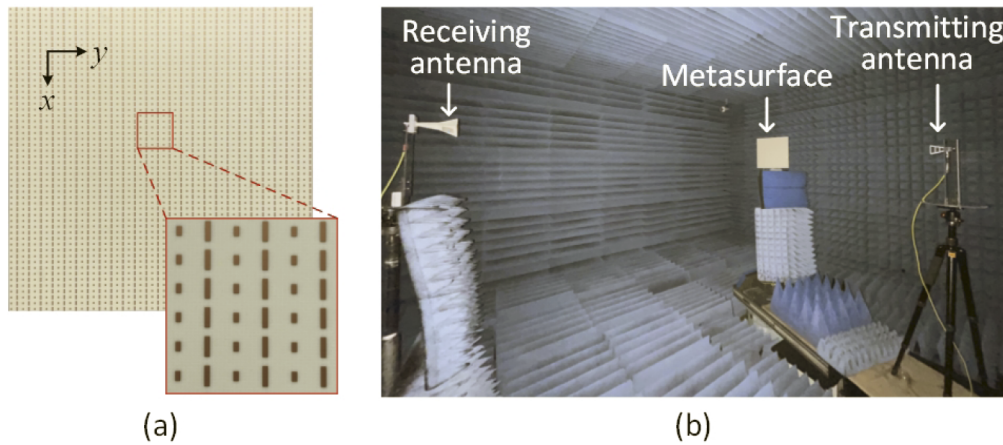


Fig. 8. (a) The fabricated metasurface. (b) The experimental setup.

the scattering patterns, the measured anomalous reflection angles agree well with the simulation results shown in Fig. 7(b), and in all cases the specular reflection is suppressed by at least 10 dB.

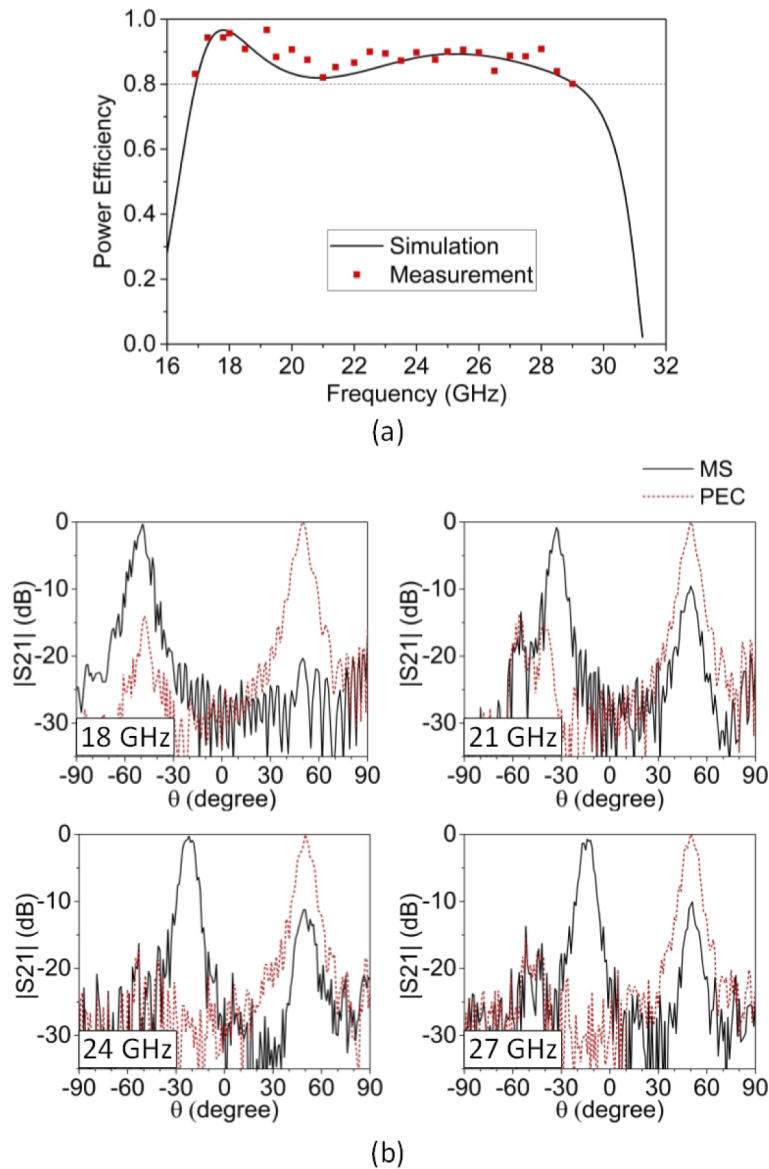


Fig. 9. Experiment results. (a) The measured anomalous reflection power efficiencies compared with the simulation results. (b) Measured scattering patterns of the metasurface compared with the those of a same-sized metallic plate at frequencies of 18 GHz, 21 GHz, 24 GHz and 27 GHz, respectively. All curves are normalized with the scattering peak of the metallic plate.

In Table 1, we compare our proposed metasurface to some finely discretized metasurface and metagrating designs in terms of the power efficiency, bandwidth, unit cell size as well as the incident and reflection/refraction angles. The power efficiency (at the design frequency) is the percentage of the incidence power coupled into the desired anomalous refraction/reflection mode, the bandwidth is the fractional frequency band within which the power efficiency reduces by

less than 1-dB from the peak efficiency. As we can see, compared to other works, our proposed design realizes a remarkable bandwidth with a satisfying efficiency at the design frequency. Additionally, due to the aggressive discretization, our proposed metasurface has a significantly enlarged unit cell size ($0.43\lambda_0$) compared to finely discretized metasurfaces (typically $0.1\lambda_0$ to $0.2\lambda_0$). The enlarged unit cell size enables us to use larger elements with multiple advantages, including larger feature sizes which are advantageous for higher frequency designs [40].

Table 1. Comparison between the proposed work and previous works

| Work | Functionality | Power efficiency | 1-dB power efficiency bandwidth | Unit cell size ^b $U_x \times U_y \times U_z$ ($\lambda_0 \times \lambda_0 \times \lambda_0$) | θ_i | θ_r^c |
|-----------|----------------------|------------------|---------------------------------|---|------------|--------------|
| [19] | Anomalous refraction | 86% | 13% ^a | 0.13×0.12×0.20 | 0° | 45° |
| [20] | | 67% | 2% ^a | 0.11×0.11×0.09 | 0° | 71.8° |
| [21] | | 80% | 6% ^a | 0.11×0.11×0.11 | 0° | 71.8° |
| [22] | | 81% | 8% | 0.13×0.13×0.11 | 0° | 30° |
| [30] | | 89% | 4.5% ^a | 0.10×0.48×0.10 | 10° | −60° |
| [23] | Anomalous reflection | 94% | 2% ^a | 0.50×0.11×0.04 | 0° | 70° |
| [24] | | 94% | 4% ^a | 0.50×0.11×0.04 | 0° | 70° |
| [31] | | 97% | 6% | 0.10×0.19×0.10 | 0° | 60° |
| [34] | | 99.98% | 35% ^a | 0.43×0.43×0.13 | 50° | −22.5° |
| This work | Anomalous reflection | 88% | 54% | 0.43×0.43×0.12 | 50° | −22.5° |

^aEstimated values from power efficiency curves shown in the papers. The 1-dB power efficiency bandwidth of work [34] is obtained by simulation using the parameters given in the paper.

^b U_y is the unit cell size in the variation direction, U_z is the metasurface thickness. For metagrating designs, we give the size of the period.

^cReflection/refraction angle at the design frequency.

4. Conclusion

In conclusion, we have investigated the bandwidth upper limit of an aggressively discretized metasurface, and demonstrated a wideband anomalous reflection metasurface with excellent (>80%) power efficiency over a large bandwidth (>50%). We established an upperbound on the bandwidth of the aggressively discretized metasurface based on a k -space consideration on the number of propagating modes. Adopting aggressive discretization of two unit cells per period enabled us to employ simple unit cells with large feature sizes, which feature robust, low-loss and broad bandwidth performances. Using the simple unit cell structure of a ground-backed dipole, we designed an anomalous reflection metasurface which achieved the specific anomalous reflection at the working frequency of 24 GHz, and maintained high-efficiency anomalous reflection over a wide bandwidth from 17–29 GHz. Simulation and experimental measurements confirm the achievement of an anomalous reflection power efficiency of higher than 80%, over a bandwidth of 53.6%, which exceeds those of previous metasurface and metagratings, including previous aggressively discretized metasurfaces. Anomalous wave redirection represents a fundamental wave manipulation functionality, which can form the building block to more complicated surfaces, including metalenses and collimation metasurfaces. We expect that, besides immediate applications in beam steering and radar cross-section (RCS) reduction, the strategy we presented hereby will help improve the bandwidth and efficiency for metasurfaces of diverse functionalities, and open doors to very versatile applications of metasurfaces.

Funding. Research Grants Council, University Grants Committee (21211619).

Disclosures. The authors declare no conflicts of interest.

Data availability. Data underlying the results presented in this paper are not publicly available at this time but may be obtained from the authors upon reasonable request.

References

1. C. L. Holloway, E. F. Kuester, J. A. Gordon, J. O'Hara, J. Booth, and D. R. Smith, "An overview of the theory and applications of metasurfaces: The two-dimensional equivalents of metamaterials," *IEEE Antennas Propag. Mag.* **54**(2), 10–35 (2012).
2. C. L. Holloway, M. A. Mohamed, E. F. Kuester, and A. Dienstfrey, "Reflection and transmission properties of a metafilm: With an application to a controllable surface composed of resonant particles," *IEEE Trans. Electromagn. Compat.* **47**(4), 853–865 (2005).
3. N. Yu and F. Capasso, "Flat optics with designer metasurfaces," *Nat. Mater.* **13**(2), 139–150 (2014).
4. A. V. Kildishev, A. Boltasseva, and V. M. Shalaev, "Planar photonics with metasurfaces," *Science* **339**(6125), 1232009 (2013).
5. S. B. Glybovski, S. A. Tretyakov, P. A. Belov, Y. S. Kivshar, and C. R. Simovski, "Metasurfaces: From microwaves to visible," *Phys. Rep.* **634**, 1–72 (2016).
6. S. Sun, Q. He, J. Hao, S. Xiao, and L. Zhou, "Electromagnetic metasurfaces: physics and applications," *Adv. Opt. Photonics* **11**(2), 380–479 (2019).
7. N. Yu, P. Genevet, M. A. Kats, F. Aieta, J.-P. Tetienne, F. Capasso, and Z. Gaburro, "Light propagation with phase discontinuities: Generalized laws of reflection and refraction," *Science* **334**(6054), 333–337 (2011).
8. C. Pfeiffer and A. Grbic, "Cascaded metasurfaces for complete phase and polarization control," *Appl. Phys. Lett.* **102**(23), 231116 (2013).
9. N. M. Estakhri and A. Alu, "Wave-front transformation with gradient metasurfaces," *Phys. Rev. X* **6**(4), 041008 (2016).
10. A. M. H. Wong and G. V. Eleftheriades, "Active Huygens' box: Arbitrary electromagnetic wave generation with an electronically controlled metasurface," *IEEE Trans. Antennas Propag.* **69**(3), 1455–1468 (2021).
11. X. Zou, G. Wang, Y. Wang, and B. Zong, "Metasurface-based coupling suppression for wideband multiple-input-multiple-output antenna arrays," *Opt. Express* **29**(25), 41643–41654 (2021).
12. P. Ang, G. Xu, and G. V. Eleftheriades, "Invisibility cloaking with passive and active huygens's metasurfaces," *Appl. Phys. Lett.* **118**(7), 071903 (2021).
13. A. Epstein and G. V. Eleftheriades, "Huygens' metasurfaces via the equivalence principle: design and applications," *J. Opt. Soc. Am. B* **33**(2), A31–A50 (2016).
14. J. P. S. Wong, M. Selvanayagam, and G. V. Eleftheriades, "Design of unit cells and demonstration of methods for synthesizing huygens metasurfaces," *Photonics Nanostruct* **12**(4), 360–375 (2014).
15. A. Epstein and G. V. Eleftheriades, "Arbitrary power-conserving field transformations with passive lossless omega-type bianisotropic metasurfaces," *IEEE Trans. Antennas Propag.* **64**(9), 3880–3895 (2016).
16. M. Chen, A. Epstein, and G. V. Eleftheriades, "Design and experimental verification of a passive Huygens' metasurface lens for gain enhancement of frequency-scanning slotted-waveguide antennas," *IEEE Trans. Antennas Propag.* **67**(7), 4678–4692 (2019).
17. M. Kalaagi and D. Seetharamdoo, "Multiangle retrodirective cascaded metasurface," *J. Appl. Phys.* **126**(10), 104901 (2019).
18. S. A. Kuznetsov, V. A. Lenets, M. A. Tumashov, A. D. Sayanskiy, P. A. Lazorskiy, P. A. Belov, J. D. Baena, and S. B. Glybovski, "Self-complementary metasurfaces for designing terahertz deflecting circular-polarization beam splitters," *Appl. Phys. Lett.* **118**(13), 131601 (2021).
19. C. Pfeiffer and A. Grbic, "Metamaterial huygens' surfaces: tailoring wave fronts with reflectionless sheets," *Phys. Rev. Lett.* **110**(19), 197401 (2013).
20. M. Chen, E. Abdo-Sánchez, A. Epstein, and G. V. Eleftheriades, "Theory, design, and experimental verification of a reflectionless bianisotropic Huygens' metasurface for wide-angle refraction," *Phys. Rev. B* **97**(12), 125433 (2018).
21. M. Chen and G. V. Eleftheriades, "Omega-bianisotropic wire-loop Huygens' metasurface for reflectionless wide-angle refraction," *IEEE Trans. Antennas Propag.* **68**(3), 1477–1490 (2020).
22. J. P. S. Wong, M. Selvanayagam, and G. V. Eleftheriades, "Polarization considerations for scalar Huygens metasurfaces and characterization for 2-d refraction," *IEEE Trans. Microw. Theory Tech.* **63**(3), 913–924 (2015).
23. V. Asadchy, A. Díaz-Rubio, S. Tcvetkova, D.-H. Kwon, A. Elsakka, M. Albooyeh, and S. Tretyakov, "Flat engineered multichannel reflectors," *Phys. Rev. X* **7**(3), 031046 (2017).
24. A. Díaz-Rubio, V. S. Asadchy, A. Elsakka, and S. A. Tretyakov, "From the generalized reflection law to the realization of perfect anomalous reflectors," *Sci. Adv.* **3**(8), e1602714 (2017).
25. Y. Saifullah, A. B. Waqas, G.-M. Yang, and F. Xu, "Multi-bit dielectric coding metasurface for em wave manipulation and anomalous reflection," *Opt. Express* **28**(2), 1139–1149 (2020).
26. Y. Shi, H. X. Meng, and H. J. Wang, "Polarization conversion metasurface design based on characteristic mode rotation and its application into wideband and miniature antennas with a low radar cross section," *Opt. Express* **29**(5), 6794–6809 (2021).
27. O. Rabinovich and A. Epstein, "Analytical design of printed circuit board (pcb) metagratings for perfect anomalous reflection," *IEEE Trans. Antennas Propag.* **66**(8), 4086–4095 (2018).

28. Y. Ra'di, D. L. Sounas, and A. Alù, "Metagratings: Beyond the limits of graded metasurfaces for wave front control," *Phys. Rev. Lett.* **119**(6), 067404 (2017).
29. D. Sell, J. Yang, S. Doshay, R. Yang, and J. A. Fan, "Large-angle, multifunctional metagratings based on freeform multimode geometries," *Nano Lett.* **17**(6), 3752–3757 (2017).
30. O. Rabinovich and A. Epstein, "Arbitrary diffraction engineering with multilayered multielement metagratings," *IEEE Trans. Antennas Propag.* **68**(3), 1553–1568 (2020).
31. A. Casolaro, A. Toscano, A. Alù, and F. Bilotti, "Dynamic beam steering with reconfigurable metagratings," *IEEE Trans. Antennas Propag.* **68**(3), 1542–1552 (2020).
32. O. Rabinovich, I. Kaplon, J. Reis, and A. Epstein, "Experimental demonstration and in-depth investigation of analytically designed anomalous reflection metagratings," *Phys. Rev. B* **99**(12), 125101 (2019).
33. X. Dong, J. Cheng, F. Fan, and S. Chang, "Low-index second-order metagratings for large-angle anomalous reflection," *Opt. Lett.* **44**(4), 939–942 (2019).
34. A. M. H. Wong and G. V. Eleftheriades, "Perfect anomalous reflection with a bipartite Huygens' metasurface," *Phys. Rev. X* **8**(1), 011036 (2018).
35. A. M. H. Wong, P. Christian, and G. V. Eleftheriades, "Binary Huygens' metasurfaces: Experimental demonstration of simple and efficient near-grazing retroreflectors for te and tm polarizations," *IEEE Trans. Antennas Propag.* **66**(6), 2892–2903 (2018).
36. C. Qi and A. M. H. Wong, "A coarsely discretized Huygens' metasurface for anomalous transmission," in *2019 IEEE Asia-Pacific Microwave Conference (APMC)* (IEEE, 2019), pp. 935–937.
37. T. Niu, W. Withayachumnankul, A. Upadhyay, P. Gutruf, D. Abbott, M. Bhaskaran, S. Sriram, and C. Fumeaux, "Terahertz reflectarray as a polarizing beam splitter," *Opt. Express* **22**(13), 16148–16160 (2014).
38. A. Pors and S. I. Bozhevolnyi, "Plasmonic metasurfaces for efficient phase control in reflection," *Opt. Express* **21**(22), 27438–27451 (2013).
39. C. Tao and T. Itoh, "Nonperiodic metasurfaces for retroreflection of te/tm and circularly polarized waves," *IEEE Trans. Antennas Propag.* **68**(8), 6193–6203 (2020).
40. C. Qi and A. M. H. Wong, "Aggressively discretized huygens' metasurface: Realizing efficient anomalous refraction with a simple design," in *2021 Fifteenth International Congress on Artificial Materials for Novel Wave Phenomena (Metamaterials)* (IEEE, 2021), pp. 350–352.